Biophysical Chemistry 266 (2020) 106437

Contents lists available at ScienceDirect

Biophysical Chemistry

journal homepage: www.elsevier.com/locate/biophyschem

Coarse-grained molecular dynamics simulations study of the conformational properties of single polyelectrolyte diblock copolymers

Mrityunjay Samanta, Srabanti Chaudhury*

Department of Chemistry, Indian Institute of Science Education and Research, Dr. Homi Bhabha Road, Pune 411008, Maharashtra, India

HIGHLIGHTS

- We study the conformational properties of single diblock polyelectrolyte chain in aqueous solution using coarse- grained Langevin dynamics simulations.
- We investigate the dependence of the basic properties such as the radius of gyration, the mean end-to-end distance and the pair correlation function on system variables such as charged residues, rigidity, dielectrics, and counterion valence for block polyelectrolytes with diblock architectures.
- Our computational studies show how the such properties of block polyelectrolytes can be tuned by varying such system properties.

GRAPHICAL ABSTRACT

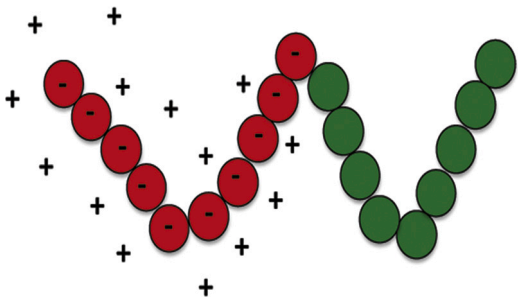

ARTICLE INFO

Keywords:
Di block polyelectrolytes
Coarse grained simulations
Conformational properties
Radius of gyration

ABSTRACT

We use coarse-grained molecular dynamics simulations to study a single di block polyelectrolyte chain in solution. We analyze the conformational properties of the chain and localization of counterions as a function of the charge fraction, backbone stiffness, Bjerrum length, and counterion valence. The interplay between the excluded-volume effects and the electrostatic interactions among charged residues leads to variation in block−−polyelectrolyte architecture. Our computational findings indicate that varying such system properties lead to nontrivial effects and can be a powerful mechanism to tune the conformational properties of block polyelectrolytes.

1. Introduction

Polyelectrolytes (PE) are the macromolecules that have ionizable groups and are used in industries and pharmaceuticals in the form of emulsifiers, adsorbents, and biological implants. These molecules dissociate to give charged polymer chains and counterions when dissolved in polar solvents like water. Due to the presence of electrostatic interactions between the charges, they behave differently from neutral polymers and display some interesting properties. The potential application in the field of biochemistry, medicine, and industries has led to recent developments in the field of polyelectrolytes. Neutral polymers have been studied for a long time and they often fail to give the real picture of what happens in biological molecules as most of them are charged, for example, DNA, RNA, and so on. The study of

* Corresponding author.
E-mail address: srabanti@iiserpune.ac.in (S. Chaudhury).

https://doi.org/10.1016/j.bpc.2020.106437
Received 8 May 2020; Received in revised form 17 July 2020
Available online 24 July 2020

polyelectrolytes is interesting as they mimic biologically relevant molecules and show how their properties change with different cellular environments (for example DNA condensation). Many factors influence the properties of polyelectrolyte solutions, such as the temperature, polymer concentration, dielectrics of the medium, size, and structure of the chain, the pH of the solution, salt concentration, and so on [1]. These variables are coupled to each other in some way or the other and their effect is difficult to interpret. This has attracted much attention in the scientific world. The structural properties of linear polyelectrolytes (eg. DNA, RNA) such as the end to end distance, the radius of gyration, the ion condensation, the radial distribution function as a function of polymer concentration, salt concentration, and valence of the added salt, the counter ion valence has been explored extensively in theoretical studies [2–4] and computer simulations [5–9]. Apart from linear polyelectrolytes, a wide range of polymerization techniques has been used for the preparation of polymers of various other architectures, such as graft copolymers, dendritic polymers, *star*-like polymers, cyclic polymers [10], and so on. A coarse-grained molecular dynamics simulation study of single *comb*-like polyelectrolytes show that conformational properties of the chain backbone with ionizable pendant chains changes with change in the fraction of side chains, length of side chains, the counterion valence, Bjerrum length, all of which will alter the strength of Coulomb interactions and the rigidity of *comb*-polyelectrolyte chains [11]. The simulation results agree qualitatively with existing experimental and theoretical studies.

Another notable class of polyelectrolytes is the block polyelectrolytes typically referred to, as block copolymers in which at least one block is a polyelectrolyte [12]. As compared to neutral block copolymers, these are charged in nature, and such charged systems find important technological applications in the field of polymer translocation. Charged tails are added to neutral molecules and such isolated charged polymers in dilute solutions could facilitate the threading of peptides across biological/solid-state nanopores [13,14]. Experimental studies show that they can alter the capture rate and can increase the residence time of such polypeptides wihtin the pore which may be required for DNA sequencing.

Computer simulation [15] serves as an important tool to study such conformational behaviors of the block polyelectrolytes that change with variation in the counterion valency, the fraction of charged residues, dielectrics, and salt concentration. In this paper, we study the conformational properties of single di block polyelectrolyte using coarse-grained molecular dynamics (MD) simulations. Details of the simulation method are given in Sec. II. Results are discussed in Sec. III, followed by conclusions in Sec. IV.

2. Model and simulation details

We start with the bead spring model of a diblock AB polymer with one block A being negatively charged and the other B being neutral. In our coarse-grained model, A and B block corresponds to the hydrophilic and hydrophobic parts respectively. Fig. 1 is a schematic illustration of the diblock polyelectrolyte chain considered in our study. We will consider a backbone chain consisting of $N = 108$ monomers and each of the charged beads along the chain carry a unit negative charge 1e. N_a is the number of charged beads and N_b is the number of neutral beads. We define a charge fraction $f = N_a/N$, where $N = N_a + N_b$ is the backbone length. In this study, the values of f are 0, 0.3, 0.4, 0.5, 0.6 and 1. Here $f = 0$ corresponds to an uncharged chain and $f = 1$ corresponds to a fully charged chain. Electroneutrality is maintained by having $N_c = N_a/Z_c$ counterions with valency Z_c. The polyelectrolyte chain is modeled by a chain of the unit charged (−1e) Lennard-Jones (LJ) beads with diameter sigma (σ) and degree of polymerization N. All the counterions are modeled as LJ particles with diameter σ. No other electrolyte is added to the solution system.

The adjacent monomer beads along the block copolymer chain are connected by FENE (finite extensible nonlinear elastic) potential

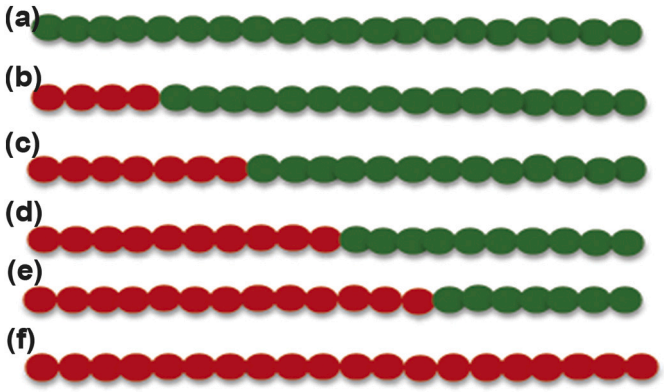

Fig. 1. Schematic illustration of the copolymer model chain. Hydrophilic charged monomers (A block) are shown in red and hydrophobic neutral beads (B block) are shown in green at different charge fraction (a) $f = 0$ (uncharged chain) (b) $f = 0.3$ (c) $f = 0.4$ (d) $f = 0.5$ (e) $f = 0.6$ and (f) $f = 1$(fully charged chain). (For interpretation of the references to colour in this figure legend, the reader is referred to the web version of this article.)

$$U_{FENE}(r) = -\frac{kR_0^2}{2} ln\left(1 - \frac{r^2}{R_0^2}\right) \quad (1)$$

where k is the spring constant and R_0 is the maximal extension. In our simulations, $k = 30\ k_BT/\sigma$ and $R_0 = 1.5\ \sigma$. The van der Waals interaction between any two non bonded beads are modeled using the shifted and truncated Lennard-Jones (LJ) potential,

$$U_{LJ}(r) = 4\varepsilon_{LJ}\left[\left(\frac{\sigma}{r}\right)^{12} - \left(\frac{\sigma}{r}\right)^{6} - \left(\frac{\sigma}{r_c}\right)^{12} + \left(\frac{\sigma}{r_c}\right)^{6}\right],\ if\ r \le r_C$$

$$= 0,\ if\ r > r_c \quad (2)$$

where r is the distance between the beads, σ is the diameter of the bead and r_c is the cut off radius. The interaction parameter ε_{LJ} for the interaction between uncharged beads is 0.3 k_BT, otherwise 1 k_BT for all other interactions. The cutoff distance r_c is set to 2.5σ for the interaction between uncharged beads which has both repulsive and attractive part of the potential and $2^{1/6}\sigma$ for all other pairwise interactions which result in a purely repulsive interaction.

The bending rigidity of chain is characterized by bond-angle potential,

$$U_{ang}(r) = k_\theta(1 - \cos(\theta - \theta_0)) \quad (3)$$

where k_θ is bending rigidity, θ is the angle between two adjacent bonds and θ_0 is the equilibrium angle between two adjacent bonds and is set to 180°. By varying the bending rigidities, the polymer chain can be made flexible or rigid. The electrostatic interaction between any two charged beads is given by the Coulomb potential,

$$U_{coul}(r) = k_BT\frac{\lambda_B q_i q_j}{r} \quad (4)$$

where q_i and q_j are the valences of the charged beads, $\lambda_B = \frac{e_0^2}{4\pi\epsilon_0\epsilon_r k_B T}$ is the Bjerrum length with e_0 being the unit charge and ε_0 and ε_r are the permittivities of vacuum and the relative dielectric constant of the implicit solvent. The Particle- Particle-Particle Mesh (PPPM) method of LAMMPS is used for calculating the Coulomb long-range electrostatic interactions [16]. Mass of all the species is taken to be 1 unit. All the measurements are done in LJ units where the fundamental quantities m, σ, ε and the Boltzmann constant (k_B) is taken to be 1. The masses, distances, energies specified are multipliers of these fundamental values. The baseline values of all the parameters and their studied range are summarized in Table 2. The whole system is put in a cubic box of length $L = 60\sigma$ with periodic boundary conditions in all three directions. Energy minimization is done before the start of the simulation.

This is to correct bad initial structures like the overlap between atoms and bond distortion. The temperature is maintained using a Langevin thermostat. The equation of motion of each of the i^{th} monomer bead of mass m is described by

$$m\ddot{r}_i = -\nabla(U_{LJ} + U_{FENE} + U_{ang} + U_{coul}) + F_i^F + F_i^R \quad (5)$$

F_i^R is the random force due to solvent atoms bumping into the particle, $F_i^F = -\eta v$ is the drag force by the solvent proportional to the velocity of the particle. The effect of solvent molecules is embedded in this friction term of the Langevin thermostat and indicates the absence of solvent molecules explicitly. The friction coefficient is set to $\eta = 1\ \tau_{LJ}{}^{-1}$ to maintain a reduced temperature of 1 unit, where $\tau_{LJ} = \sigma(m/\epsilon_{LJ})^{1/2}$ is the standard LJ unit of time. F_i^R is the random force with a zero mean $\langle F_i^R(t)\rangle = 0$ and satisfies the fluctuation-dissipation theorem $\langle F_i^R(t)F_j^R(t')\rangle = 6\eta k_B T\delta_{ij}\delta(t-t')$ The open-source software LAMMPS is used to perform simulations [17]. NVE integration is used to update the position and velocity of atoms with a time step equal to $0.01\tau_{LJ}$. The system is equilibrated for 3×10^6 time steps and the equilibration of the system is observed by the convergence of R_g. Simulations are run for 6×10^6 time steps and the data was saved every 1000 time steps to analyze the desired quantities.

3. Results and discussion

3.1. Radius of gyration

To calculate the conformational behavior of a diblock polyelectrolyte chain, we obtain the backbone gyration radius, $\langle R_g{}^2\rangle$ defined as

$$\langle R_g^2\rangle = \frac{1}{N}\left\langle \sum_{i=1}^{N} (r_i - r_{CM})^2 \right\rangle \quad (6)$$

where the position of the center-of-mass (COM) of the chain,

Table 1
Mean of radius of gyration and the standard error at (a) with Coulomb and Coulomb + LJ interactions (b) different counter ion valency Zc, (c) bending rigidity k_θ and (d) Bjerrum length λ_B for different charge fractions *f*.

The radius of gyration is the mean of 5 independent runs and the error associated with it is the standard error given by SE= $\frac{\sigma}{\sqrt{N}}$, where the standard deviation $\sigma = \frac{\sum(x_i-\bar{x})^2}{\sqrt{N-1}}$, *N* is the number of independent runs and $\bar{x}$ is the mean. Here $N = 5$.

(a)

	f = 0.3		f = 0.4		f = 0.5		f = 0.6		f = 1	
	Mean	SE	Mean	SE	Mean	SE	Mean	SE	Mean	SE
Coulomb	85.40	1.91	110.08	3.79	154.31	5.10	198.19	3.79	341.28	4.14
Coulomb + LJ	63.32	1.40	96.28	1.68	137.46	2.61	177.61	2.82	341.30	4.13

(b)

	f = 0.3		f = 0.4		f = 0.5		f = 0.6		f = 1	
Z_C	Mean	SE	Mean	SE	Mean	SE	Mean	SE	Mean	SE
1	58.07	0.79	95.15	1.64	137.46	2.61	166.51	3.08	341.30	4.13
2	51.38	1.52	69.14	1.27	91.75	0.93	99.18	2.24	178.67	4.74
3	46.02	1.07	52.54	1.88	59.84	0.61	63.24	2.63	81.95	1.76

(c)

	f = 0		f = 0.3		f = 0.4		f = 0.5		f = 0.6		f = 1	
k_θ	Mean	SE	Mean	SE	Mean	SE	Mean	SE	Mean	SE	Mean	SE
0	35.64	1.04	63.32	1.40	96.28	1.68	137.46	2.61	177.61	2.82	341.30	4.13
3	74.98	4.39	119.19	2.79	148.01	3.49	188.14	4.67	245.17	7.27	446.90	5.32
5	126.35	6.01	160.30	8.27	181.28	3.88	242.21	6.47	304.63	7.93	463.47	4.70
7	201.72	21.10	212.77	8.53	261.11	13.16	267.86	11.50	323.22	5.57	482.86	11.20
10	270.50	14.23	283.86	11.65	295.15	17.95	297.31	21.93	349.36	24.75	507.53	6.71

(d)

	f = 0		f = 0.3		f = 0.4		f = 0.5		f = 0.6		f = 1	
λ_B	Mean	SE	Mean	SE	Mean	SE	Mean	SE	Mean	SE	Mean	SE
4	57.02	1.07	78.04	3.05	99.61	4.07	99.61	4.07	125.49	3.71	223.69	10.27
3.03	60.43	2.13	87.89	1.51	111.06	2.42	111.06	2.42	142.59	3.39	257.20	2.03
2	65.67	0.93	94.41	1.95	131.93	3.04	131.93	3.04	167.48	1.54	292.75	3.70
1.52	65.10	2.55	98.48	1.08	136.02	2.72	136.02	2.72	184.55	2.52	318.12	4.60
1	63.32	1.40	96.28	1.68	137.46	2.61	137.46	2.61	177.61	2.82	341.30	4.13
0.67	61.91	0.95	86.90	3.18	130.24	3.39	130.24	3.39	173.21	2.38	340.52	3.95
0.5	59.54	0.93	84.10	1.45	118.09	2.26	118.09	2.26	169.79	1.77	321.11	3.46
0.33	55.90	1.18	74.84	0.62	106.71	2.57	106.71	2.57	145.60	2.32	283.88	3.37
0.25	55.08	1.18	70.04	1.57	96.86	3.02	96.86	3.02	130.14	3.10	254.74	2.28

Table 2
List of system parameters with their baseline values along with the explored parameter range.

Parameter	Baseline value	Parameter range explored
F	0.5	0–1
λ_B	1	0.3–4 σ
K_θ	0	0–10 k_BT
Z_C	$1e^-$	1 - $3e^-$

$r_{CM} = \frac{1}{N}\sum_{i=1}^{N} r_i$, N is the number of backbone beads and r_i is the position vector of the i^{th} bead. Angular brackets indicate the averaging over all the chain configurations. The dependence of the radius of gyration on the charged chain fraction, the bending rigidity, the dielectric constant, and the valency of the counterion is discussed below. This dependence is a concerted effect of the electrostatic attraction between the polymer beads and counterions, the electrostatic repulsion between polymer beads, the excluded volume interaction between polymer beads, and the configurational entropy of polymer chains. The radius of gyration mentioned in all the plots below is the mean of 5 independent runs and the error associated with it (standard error) is shown in Table 1.

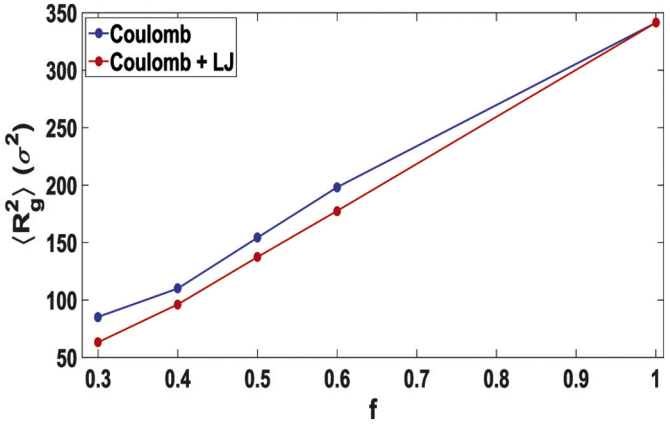

Fig. 2. Changes of the radius of gyration for diblock copolymers as a function of f in the presence of monovalent counterions (red line). The blue line shows the pure electrostatic contributions to the Rg by subtracting the excluded-volume effects from Rg values presented in the red curve. The other system parameters for the simulations are the baseline values given in Table 2. (For interpretation of the references to colour in this figure legend, the reader is referred to the web version of this article.)

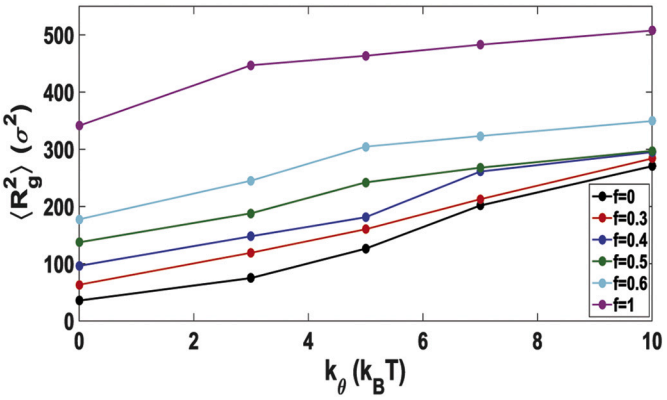

Fig. 4. Effect of k_θ on the R_g of the diblock polyelectrolyte at different charged chain fractions f. The other system parameters for the simulations are the baseline values given in Table 2.

3.1.1. *Effect of charged chain length segment*

Fig. 2 shows the results for R_g as a function of f obtained for a charged diblock polyelectrolyte at zero bending rigidity. This implies that conformational changes will originate only from the excluded-volume interactions and electrostatic effects. The R_g increases with the increase in f due to the increase in electrostatic repulsions among the charged beads that cause greater stretching along the backbone.

We observe that the R_g is higher for pure electrostatic contributions than when both electrostatic and excluded volume effects are considered. This is due to the excluded volume effects originating from interactions between neutral beads. The LJ potential between the uncharged monomer beads has both attractive and repulsive interactions whereas the LJ potential for all other pairwise interactions is purely repulsive. The attractive part of LJ tends to bring the neutral beads closer and hence the overall R_g decreases. As f increases, the number of uncharged beads decreases, and hence the effect of the excluded volume interactions in determining R_g decreases.

At $f = 1$, there are no uncharged beads to feel the extra LJ potential. Hence the values of the R_g in both cases are similar.

Fig. 3 shows the simulation snapshots of a diblock-polyelectrolyte chain at different f values [18]. The conformational behavior observed in these images is in line with the conformational characteristics reported in Fig. 2.

3.1.2. *Effect of bending rigidity*

The R_g is calculated for different bending rigidities k_θ at different charge fraction f as shown in Fig. 4. As the bending rigidity increases, the R_g value increases faster for lower f values and remains almost

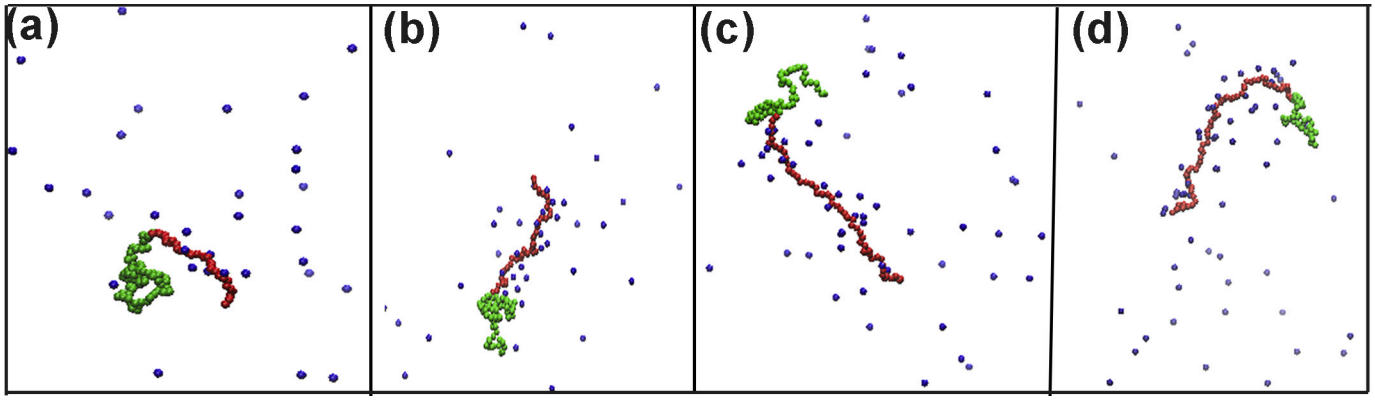

Fig. 3. The simulation snapshots [18] at baseline parameter values upon increasing the charge fraction f (a) f = 0.3 (b) f = 0.4 (c) f = 0.5 (d) f = 0.6. Hydrophobic uncharged beads B are shown in green, hydrophilic charged beads A are represented by red and the counterions are shown by blue. (For interpretation of the references to colour in this figure legend, the reader is referred to the web version of this article.)

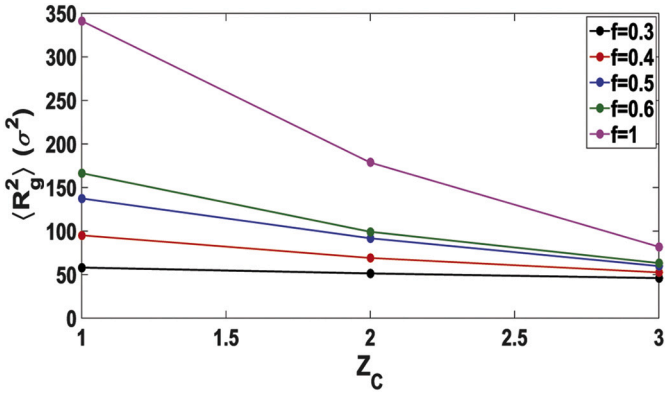

Fig. 5. The radius of gyration as a function of counterion valence Z_C at different charge fractions *f*. The other system parameters for the simulations are the baseline values given in Table 2.

constant at higher *f* values. Two factors come into play: the intra-chain bead repulsions and stiffness of the chain. An increase in repulsion between the chain beads causes the chain to spread out and so does the stiffness of the chain increases. At lower *f* values, the number of charged beads is less and hence the overall repulsion among the chain beads is low. So the increase in the bending rigidity causes an increase in the R_g values. At higher *f* values, with the increase in the number of charged beads, the intra bead repulsions become stronger. This causes the chain to spread out more and the increase in bending rigidity has minimal effect on the R_g since the chain is already stiff due to such repulsions.

3.1.3. Effect of counterion valency

The change in R_g with the change in the counterion valence Z_C for a chain with different *f* values is shown in Fig. 5. The number of counter ions N_c is varied to maintain electroneutrality $N_c = N_a/Z_c$ for different charged fraction values. The decrease of R_g with an increase of the valence of counterions is due to the increased screening by higher valent cations that result in a decrease of electrostatic repulsion between the charged chain beads. The increased electrostatic attraction between charged polymer beads and the high valent counterions lead to more localization of counterions closer to the polyelectrolyte chain. This leads to the formation of globular structures around those counterions. The reduction in R_g is more for chains with higher values of *f* due to an increase in the electrostatic contribution to the R_g at high values of *f*. This is also manifested in Fig. 6 where we show the simulation snapshots of PE copolymers as a function of different counterion valences at a given charge fraction [18].

3.1.4. Effect of electrostatic interaction strength

We study how the R_g values are influenced by varying the Bjerrum length λ_B for different chain fraction *f*. Here λ_B is altered by changing the strength of electrostatic interactions at a constant temperature. The R_g has a nonmonotonic dependence on the λ_B for all values of *f* (See Fig. 7). Initially with an increase in λ_B, the chain extends due to the increase in the electrostatic repulsion. With further increase in λ_B there is a strong localization of counterions near the chain. This screens the anionic charges on the chain beads and lowers the effective electrostatic repulsion thereby decreasing the R_g values. It indicates that increasing the charge fraction will not always lead to the chain elongation with an increase in R_g and is also sensitive to the strength of electrostatic interactions. At low values of *f*, the change in R_g concerning the Bjerrum length is less significant because of the lower electrostatic repulsion among the charged beads.

4. Mean square end-to-end distance

To calculate the conformational behavior of a diblock polyelectrolyte chain, we calculate the mean square end-to-end distance $< R_e^2 >$ defined as

$$\langle R_e^2 \rangle = \langle (r_N - r_1)^2 \rangle \tag{7}$$

In Appendix A, we show the dependence of $\langle R_e^2 \rangle$ on the bending rigidity, the dielectric constant, and the valency of the counterions. The conformational properties as inferred both from R_g and R_e calculations follow the same trend.

5. Radial distribution function

To obtain a quantitative measure of the distribution of counterions around the polyelectrolyte chain, we calculate the radial distribution function (RDF) that describes the localization of the counterions around the polymer beads. In general, the RDF, $g_{A\text{-}B}(r)$ is defined as the probability of finding a particle A from a reference particle B at a specific radial distance, *r*. Here it describes the probability of finding a counterion in a shell of polymer bead of radius *r*. It is defined as:

$$g_{A-B}(r) = \frac{V}{4\pi^2 N_A N_B} \sum_{i=1}^{N_A} \sum_{j=1}^{N_B} \langle \delta(r - r_{ij}) \rangle \tag{8}$$

where N_A and N_B represent the total number of A and B particles.

In Fig. 8, we show the RDF for charged monomer (p) and the counterion(c) as a function of *f*. For all charge fractions *f*, g(r) peaks at almost the same value of *r* but the height of peak decreases with the increase in *f*. At lower values of *f*, the chain is in a coiled state and the

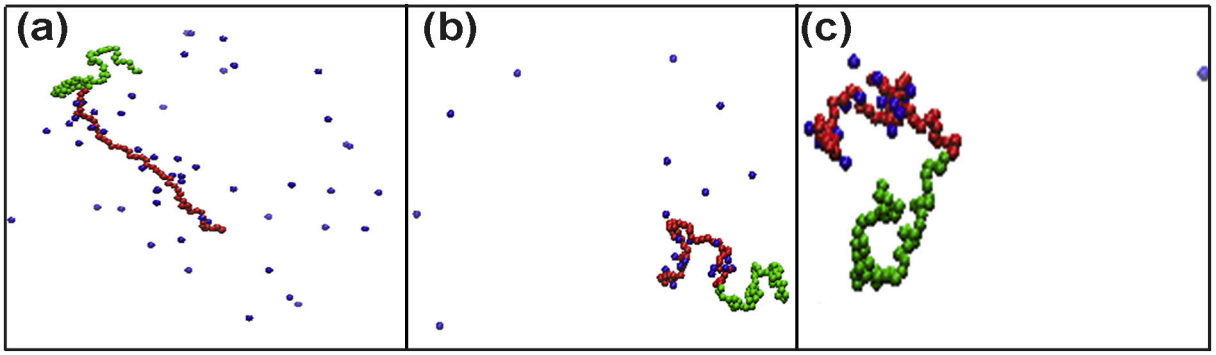

Fig. 6. Simulation snapshots [18] at different counter ion valencies (a) $Z_C = 1$, (b) $Z_C = 2$ and (c) $Z_C = 3$. Each column has the same charge fraction, f = 0.5. Hydrophobic uncharged beads B are shown in green, hydrophilic charged beads A are represented by red and the counterions are shown by blue. (For interpretation of the references to colour in this figure legend, the reader is referred to the web version of this article.)

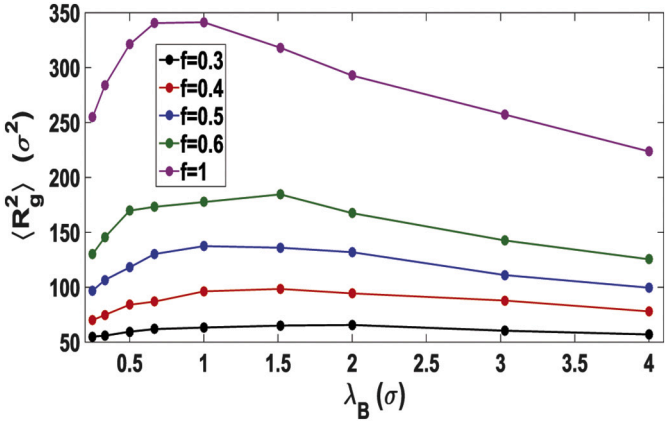

Fig. 7. R_g values as a function of Bjerrum length at different charge fractions. The other system parameters for the simulations are the baseline values given in Table 2.

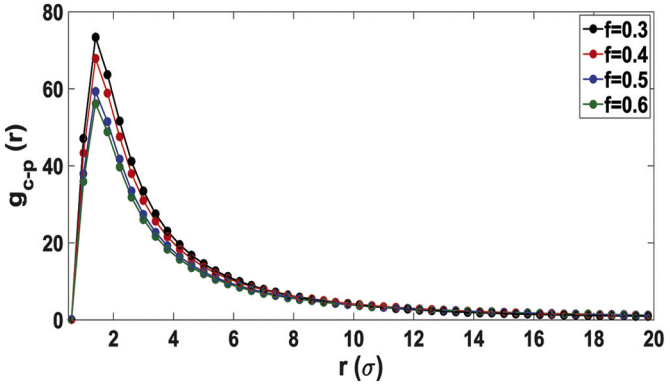

Fig. 8. The changes in charged monomer(p) – counterion(c) RDF, $g_{c\text{-}p}(r)$, at different charge fraction. The system parameters for the simulations are the baseline values given in Table 2.

counterions are more localized than at higher f values where the counterions are more spread out in the solution. As f decreases, the number of counterions around the charged ions on the block polymer increases and thus the magnitude of $g_{c-p}(r)$ increases.

These observations show that the architectural variation in diblock polyelectrolytes plays an important role in the distribution of counterions around the polymer.

6. Conclusion

In this work, we use coarse-grained molecular dynamics simulations to study the non-trivial effects of different parameters such as the charged fraction of the chain, counter ion valence, the dielectric constant, and the bending rigidity on the conformational properties of diblock polyelectrolytes. We look at specifically few important quantities such as the radius of gyration, the mean end-to end distance and the other one is the pair correlation function. The conformational behaviors of diblock polyelectrolytes captured in our coarse-grained simulation model follow the same qualitative trend as those reported from coarse-grained simulations for another kind of copolymers such as the *comb*-like polyelectrolytes or end-grafted flexible diblock copolymers studied by using Monte Carlo simulation [19,20]. The conformational characteristics such as the collapse of the block polyelectrolyte chain that can be induced by varying either the long-range electrostatic interactions (dielectrics) or the distribution of the counterions (charged fractions, counter ion valence) has been analyzed. Our results show the response of block polyelectrolytes to stimuli such as charged chain fractions, counterion valence, bond stiffness that can tune their morphological properties. This agrees qualitatively with extensive experimental studies where it has been shown that the composition, the number of repeating units are important parameters that can impact the geometry [21] and determine the morphologies of diblock copolymers [22]. In this study, we have observed that at different values of charge fractions there are different conformations of copolymers due to varying interaction among the hydrophobic and the hydrophilic part. This can be extended to study the formation of nanodiscs where different copolymers interact with the lipid bilayer membrane to destabilize it, leading to the formation of polymer nanodiscs of different sizes driven by the hydrophobic effect [23,24].

Coarse graining model can lead to a loss in some details. For example, the internal structure of the chain represented by the beads remains the same thereby lacking the chemical specificity. In real conditions, macromolecules like protein can have changes in the internal structure due to interaction between atoms, dimerization, docking, interaction with other biomolecules or undergo some transitions like folding-unfolding. All-atom simulations can address these concerns but are limited by computing power and algorithms used [25]. However such problems can be addressed to a large extent by coarse-grain models by using effective force fields. Also such single chain systems are also not constrained in space due to periodic boundary conditions which may lead to greater stability than is expected in real experimental conditions. In biological conditions chain properties may be subject to many constraints like potentials from the surfaces as in the case of docking with the enzymes or motion through pores. Therefore the conformational properties may not apply there. Nevertheless, many such constraints can be modeled through the various variables in the system like the bending rigidity and dielectric constant without explicitly constructing those surfaces.

Declaration of Competing Interest

The authors declare that they have no known competing financial interests or personal relationships that could have appeared to influence the work reported in this paper.

Acknowledgments

The authors would like to acknowledge DAE-BRNS (37(2)/14/08/2016-BRNS/37022), SERB CRG/2019/000515, and IISER Pune for funding. M. S thanks IISER Pune and INSPIRE for fellowship. The authors acknowledge C-DAC Pune for computational facilities. We thank Dr. Bappa Ghosh for useful discussions and comments regarding the paper.

Appendix A

The conformation of block polyelectrolytes can also be characterized by the mean-square end-to-end distance, defined by Eq. (7).

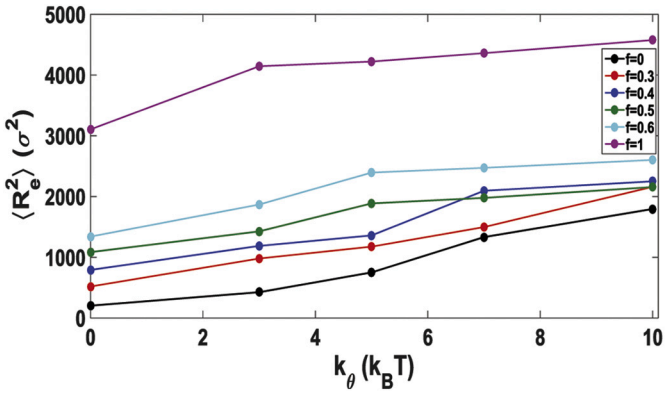

Fig. A.1. Effect of k_θ on the R_e of the diblock polyelectrolyte at different charged chain fractions *f*. The other system parameters for the simulations are the baseline values given in Table 2.

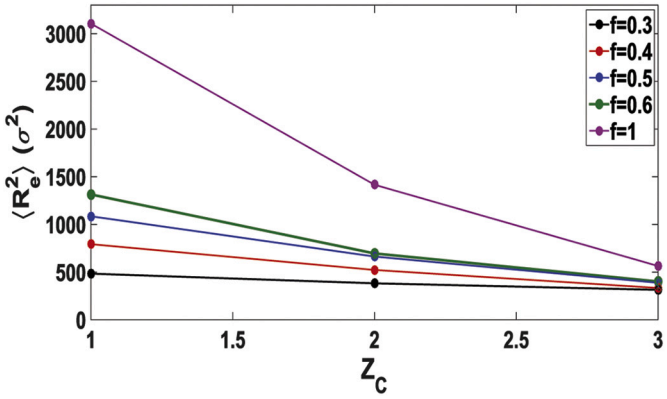

Fig. A.2. R_e as a function of counterion valence Z_C at different charge fractions *f*. The other system parameters for the simulations are the baseline values given in Table 2.

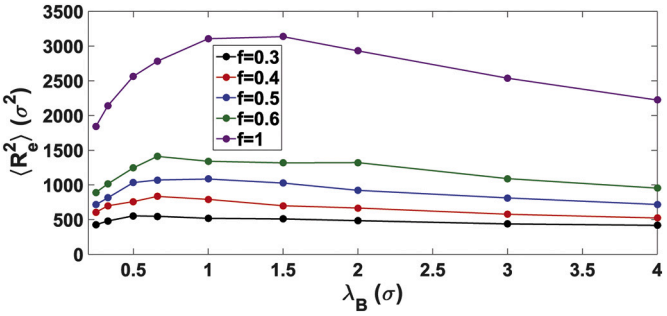

Fig. A.3. R_e values as a function of Bjerrum length at different charge fractions. The other system parameters for the simulations are the baseline values given in Table 2.

References

[1] M. Muthukumar, 50th anniversary perspective: a perspective on polyelectrolyte solutions, Macromolecules 50 (2017) 9258.

[2] A.V. Dobrynin, Theory and simulations of charged polymers: from solution properties to polymeric nanomaterials, Curr. Opin. Colloid Interface Sci. 13 (2020) 376–388.

[3] A.V. Dobrynin, R.H. Colby, M.S. Rubinstein, Scaling theory of polyelectrolyte solutions, Macromolecules 28 (1859 – 1871).

[4] A.V. Dobrynin, M. Rubinstein, Theory of polyelectrolytes in solutions and at surfaces, Prog. Polym. Sci. 30 (2005) 1049–1118.

[5] M.J. Stevens, K. Kremer, The nature of flexible linear polyelectrolytes in salt free solution: a molecular dynamics study, J. Chem. Phys. 103 (1995) 1669.

[6] Q. Liao, A.V. Dobrynin, M. Rubinstein, Molecular dynamics simulations of polyelectrolyte solutions: nonuniform stretching of chains and scaling behavior, Macromolecules 36 (2003) 3386–3398.

[7] J.-M.Y. Carrillo, A.V. Dobrynin, Polyelectrolytes in salt solutions: molecular dynamics simulations, Macromolecules 44 (2011) 5798–5816.

[8] S. Liu, K. Ghosh, M. Muthukumar, Polyelectrolyte solutions with added salt: a simulation study, J. Chem. Phys. 119 (2011) 1813.

[9] C. Rakwoo, A. Yethiraj, Brownian dynamics simulations of polyelectrolyte solutions with divalent counterions, J. Chem. Phys. 118 (2003) 1135.

[10] G. Riess, Micellization of block copolymers, Prog. Polym. Sci. 28 (2003) 1107–1170.

[11] M. Ghelichi, M.H. Eikerling, Conformational properties of comb-like polyelectrolytes: a coarse-grained md study *J*, Phys. Chem. B 120 (2016) 2859.

[12] S. Yang, A. Vishnyakov, A.V. Neimarka, Self-assembly in block polyelectrolytes, J. Phys. Chem. B 134 (2011) 054104.

[13] A. Asandei, M. Chinappi, J.K. Lee, C. Ho Seo, L. Mereuta, Y. Park, T. Luchian, Placement of oppositely charged aminoacids at a polypeptide termini determines the voltage-controlled braking of polymer transport through nanometer-scale pores, Sci. Rep. 5 (2015) 10419.

[14] S. Biswas, W. Song, C. Borges, S. Lindsay, P. Zhang, Click addition of a DNA thread to the N-termini of peptides for their translocation through solid-state nanopores, ACS Nano 9 (2015) 9652–9664.

[15] K. Tai, Conformational sampling for the impatient, Biophys. Chem. 107 (2004) 213–220.

[16] T. Darden, D. York, L. Pedersen, Particle mesh Ewald: an N·log(N) method for Ewald sums in large systems, J. Chem. Phys. 98 (1993) 10089–10092.

[17] S. Plimpton, Fast parallel algorithms for short-range molecular dynamics, J. Comput. Phys. 117 (1995) 1–19.
[18] W. Humphrey, A. Dalke, K. Schulten, Vmd - visual molecular dynamics, J. Mol. Graph. 14 (2020) 33–38.
[19] M. Kosmas, C. Vlahos, A theoretical study of conformational properties of dendritic block copolymers of first generation, J. Chem. Phys. 125 (2006) 094908.
[20] H. Hong Li, B. Gong, C.-J. Qian, C.-Y. Li, J.-H. Huang, M.-B. Luo, Simulation of conformational properties of end-grafted Diblock copolymers, RSC Adv. 4 (2014) 27393–27398.
[21] J. Zarzar, W. Shatz, N. Peer, R. Taing, B. McGarry, Y. Liu, D.G. Greene, Impact of polymer geometry on the interactions of protein-peg conjugates, Biophys. Chem. 236 (2018) 22–30.
[22] H. Feng, X. Lu, W. Wang, N.-G. Kang, J.W. Mays, Block copolymers: synthesis, self-assembly, and applications, Polymers 9 (2017) 494.
[23] B.R. Sahoo, T. Genjo, K.C. Moharana, A. Ramamoorthy, Self-assembly of polymer-encased lipid nanodiscs and membrane protein reconstitution, J.Phys. Chem. B 123 (2019) 4562–4570.
[24] M. Xue, L. Cheng, I. Faustino, W. Guo, S. Marrink, Molecular mechanism of lipid nanodisk formation by styrene-maleic acid copolymers, Biophys. J. 115 (2018) 494–502.
[25] P. Faccili, A.A. Beccara, Computing reaction pathways of rare biomolecular transitions using atomistic force-fields, Biophys. Chem. 208 (2016) 62–67.